Article:

Saha, S. orcid.org/0000-0001-7106-2936, Moon, S. orcid.org/0000-0001-5207-1781, Brown, N.D. et al. (5 more authors) (2021) Holocene depositional history inferred from single-grain luminescence ages in southern California, North America. ESS Open Archive.

https://doi.org/10.1002/essoar.10506324.1

Holocene depositional history inferred from single-grain luminescence ages in southern California, North America.

Sourav Saha[1], Seulgi Moon[2], Nathan D Brown[3], Edward Rhodes[4], Katherine M. Scharer[5], Devin McPhillips[6], Sally F. McGill[7], and Bryan A Castillo[7]

[1]University of California
[2]University of California Los Angeles
[3]University of California, Berkeley
[4]University of Sheffield
[5]United States Geological Survey
[6]US Geological Survey
[7]California State University, San Bernardino

November 24, 2022

Abstract

Significant sediment flux and deposition in a sedimentary system are influenced by climate changes, tectonics, lithology, and the sedimentary system's internal dynamics. Identifying the timing of depositional periods from stratigraphic records is a first step to critically evaluating the controls of sediment flux and deposition. Here, we show that ages of single-grain K-feldspar luminescence subpopulations may provide information on the timing of previous major depositional periods. We analyzed 754 K-feldspar single-grains from 17 samples from the surface to ˜9 m-depth in a trench located downstream of the Mission Creek catchment. Single-grain luminescence subpopulation ages significantly overlap at least eight times since ˜12.0 ka indicating a common depositional history. These depositional periods correspond reasonably well with the wetter climate periods based on hydroclimatic proxies from nearby locations. Our findings imply a first-order climatic control on sediment depositional history in southern California on a millennial timescale.

Holocene depositional history inferred from single-grain luminescence ages in southern California, North America

Sourav Saha[1], Seulgi Moon[1], Nathan D. Brown[2], Edward J. Rhodes[1,3], Katherine M. Scharer[4], Devin McPhillips[4], Sally F. McGill[5], and Bryan A. Castillo[5]

[1] Earth, Planetary, and Space Sciences, University of California, Los Angeles, USA,

[2] Department of Earth and Environmental Sciences, University of Texas, Arlington, USA,

[3] Department of Geography, University of Sheffield, Sheffield, UK,

[4] Earthquake Science Center, U.S. Geological Survey, Pasadena, USA

[5] Department of Geological Sciences, California State University, San Bernardino, USA

Corresponding authors: Sourav Saha (sahasv@ucla.edu) and Seulgi Moon (sgmoon@ucla.edu)

Key Points:

- Single-grain luminescence ages reveal at least eight major depositional periods in the lower Mission Creek catchment during ~12.0–0.6 ka.
- These depositional periods correspond reasonably well with the wetter periods in southern California based on paleoclimatic proxies.
- The average interval between intermittent depositional periods increases from the Late Holocene (~0.7 ka) to the Mid-Holocene (~1.6 ka).

Abstract

Significant sediment flux and deposition in a sedimentary system are influenced by climate changes, tectonics, lithology, and the sedimentary system's internal dynamics. Identifying the timing of depositional periods from stratigraphic records is a first step to critically evaluating the controls of sediment flux and deposition. Here, we show that ages of single-grain K-feldspar luminescence subpopulations may provide Information on the timing of previous major depositional periods. We analyzed 754 K-feldspar single-grains from 17 samples from the surface to ~9 m-depth in a trench located downstream of the Mission Creek catchment. Single-grain luminescence subpopulation ages significantly overlap at least eight times since ~12.0 ka indicating a common depositional history. These depositional periods correspond reasonably well with the wetter climate periods based on hydroclimatic proxies from nearby locations. Our findings imply a first-order climatic control on sediment depositional history in southern California on a millennial timescale.

Plain Language Summary

Various environmental factors such as climate, tectonics, rock types, and internal sedimentary processes may influence sediment generation, delivery, and deposition over thousand-year timescales. To understand what controls sedimentation, we first seek to understand when periods of significant sediment transport and deposition have occurred in the past. Previous studies have shown that luminescence signals from individual sand grains may preserve Information on past sunlight exposure (luminescence bleaching) and burial (luminescence regeneration) history. In this case, the overlapping ages of individual sand grain subpopulations may represent the timing of significant depositional periods that occurred prior to (and upstream of) the current deposit.

We collected 17 samples from a trench located on the Banning fault of the San Andreas Fault system in southern California. Using these samples, we identified at least eight Holocene overlapping luminescence ages of single-grain subpopulations. These subpopulation ages broadly match the periods of substantially wetter climate in the last 12,000 years, indicating a first-order climatic influence on sediment transport and depositional history in southern California.

1 Introduction

The geologic history of sediment flux and deposition is influenced by changes in external environmental factors such as climate and tectonics and intrinsic factors such as lithology and the sedimentary system's internal dynamics (Romans et al., 2016; Toby et al., 2019). Due to the complexity of these various factors, it is challenging to identify the first-order control, whether external (allogenic) or internal (autogenic), on sediment generation, transport, and downstream deposition (Armitage et al., 2011, 2013). In addition, how these signals are recorded in stratigraphic archives and geomorphic landforms over various geologic timescales is still poorly understood (Gray et al., 2019; Caracciolo et al., 2020). This is particularly challenging since the studies often rely on spatially and/or temporally incomplete stratigraphic sequences (Jerolmack and Paola, 2010; Miall, 2015) or suffer from poor chronological constraints (Owen et al., 2014 and references therein). For example, researchers still debate whether the significant alluvial fan depositions in the American Southwest took place during relatively dry periods, especially during glacial to interglacial transitions with reduced soil moisture and vegetation cover (e.g., Bull, 1977, 1991, 2000; Wells et al., 1987, 1990; Spelz et al., 2008) or during the wetter periods due to enhanced runoff and sediment transport capacity (e.g., Ponti, 1985; Harvey et al., 1999a,b;

Inman and Jenkins 1999; Warrick and Milliman 2003; Miller et al., 2010; Kirby et al., 2012, 2014; Owen et al., 2014).

Recent studies have shown that single-grain luminescence signals can be used effectively to examine variable past sunlight exposure (luminescence bleaching) and burial (luminescence regeneration) history (Smedley et al., 2015; Gray et al., 2018, 2019 and references therein). Before burial, some grains may experience sunlight exposure, and their luminescence clock is reset to zero (Wintle, 1997; Duller, 2004; Lian and Roberts, 2006; Rhodes, 2011). However, other grains may suffer insufficient sunlight exposure depending on the bleachability of the targeted luminescence signal (feldspar signals bleach slower than quartz signals) and transport conditions (Fuchs and Owen, 2008; Gray et al., 2019; Brown, 2020). For example, a grain traveling within turbulent muddy water may experience very dim attenuated sunlight, whereas windblown grains often see a bright, full spectrum of sunlight. For feldspar grains in fluvial settings, complete signal resetting prior to burial is not guaranteed (Wallinga, 2002; Colarossi et al., 2015; Gliganic et al., 2017; Brill et al., 2018). In that case, we can examine the age distribution of feldspar grains to estimate the most recent and perhaps previous depositional events, assuming that a portion of grains was fully bleached and the rest was not bleached at all before each burial event, respectively (e.g., Gliganic et al., 2015, 2016; Rhodes, 2015).

In Figure 1a, we present a simple schematic of nested alluvial fans and a hybrid (fan and axial valley wash) depositional setting. Assuming that only a fraction of feldspar grains are bleached during any single flood, other grains will retain a prior depositional age, and we can use the multiple ages of single-grain subpopulations (i.e., different colors of stippling in discs representing multiple single-grain ages in Figure 1a) to represent the most recent as well as older depositional ages. If a sedimentary system is driven by significant external environmental perturbation, large burial events may be preserved in distant deposits in multiple stratigraphic units in a well-connected sediment routing system (Figure 1b). As such, single-grain luminescence subpopulation ages from different deposits are expected to show multiple overlapping ages likely driven by the shared perturbations (e.g., E1, E2, and E3 events in Figure 1b). If burial events are site-specific and not system-wide, likely due to autogenic processes, single grain subpopulation ages from different deposits may be unrelated (Figure 1c).

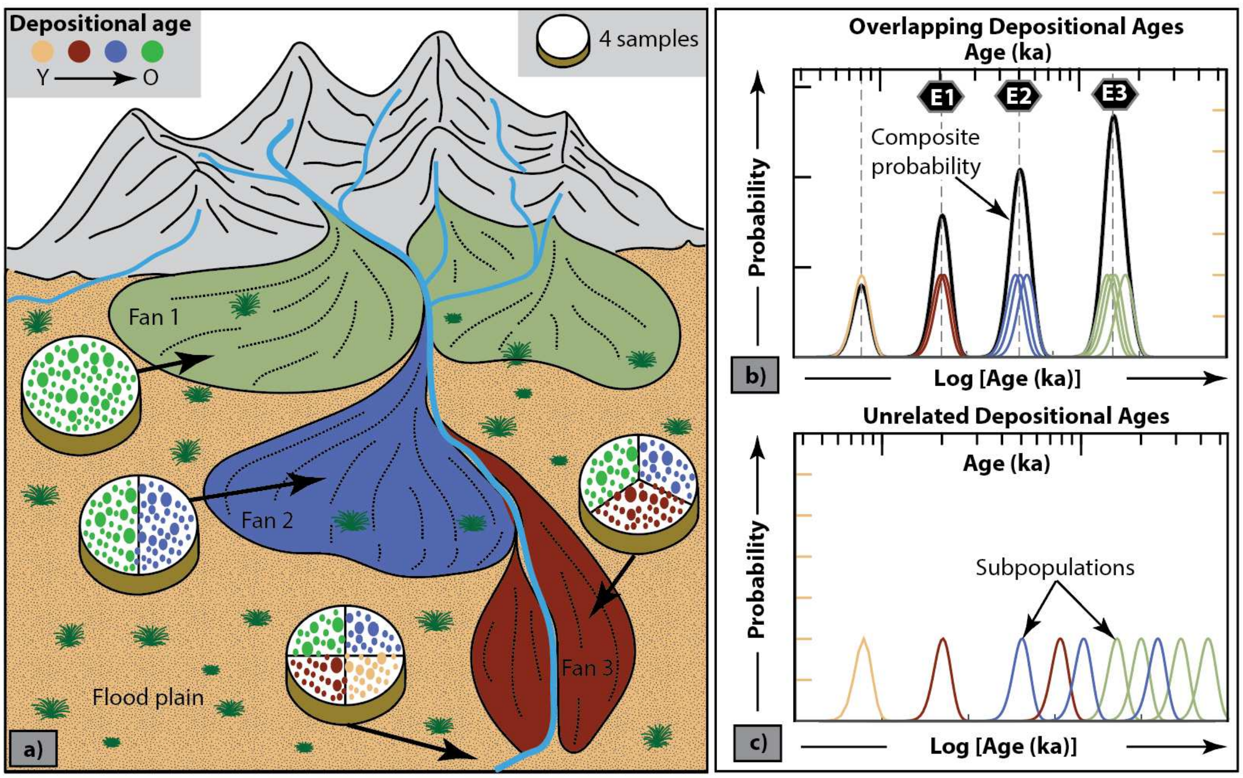

Figure 1. (a) Schematic representation of a simplified sediment routing system and expected age distribution of single-grain luminescence subpopulations. Different colors of stippling mounted on discs represent multiple single-grain luminescence ages from three distinct fans and the floodplain (arrows show the samples' location). Different proportions of distinct single-grain ages are expected if samples are not completely bleached before their burial. (b) A hypothetical example of three overlapping depositional events (i.e., E1, E2, E3) derived from ten subpopulations determined from four samples collected at distinct fans and the floodplain. This is expected if the subpopulations share common sediment routing history. Composite probability (black line) is presented for the closely overlapped

subpopulations, with the dashed line highlighting the mode. The y-axes show probability corresponding to log[age(ka)] (Galbraith, 2011; see section 2.3). Note that 10% relative errors are used for the hypothetical single-grain subpopulations in log-scale, resulting in narrower composite probability peaks for older ages. (c) An alternative scenario where the subpopulations do not overlap at a specific time, likely indicating either unrelated or more complex site-specific stochastic depositional histories.

To test this hypothesis, we examine luminescence ages in single-grain K-feldspars using the post-Infrared Infrared Stimulated Luminescence (p-IR IRSL; Reimann et al., 2012; Rhodes, 2015) technique from seventeen sediment samples collected from the surface to ~9 m depth at the Banning fault trench site, southern California, located downstream of the Mission Creek catchment (Figure 2). We first identified significant depositional periods shared in multiple samples from distinct stratigraphic units. Then, we compared these depositional periods with the regional hydroclimatic proxies from nearby sites in southern California.

2 Methods

2.1 Sample Collection and Preparation

Seventeen sediment samples were collected from a ~92 m-long and ~8 m-deep N–S trending trench (Figures 2, S1; Castillo et al., 2020), which is located in a hybrid depositional environment (Figure 2; e.g., Miller et al., 2010). The trench is located ~18 km downstream from the oldest alluvial fan's apex at the Mission Creek catchment on the Banning strand of the San Andreas Fault (SAF). The upstream catchment represents a typical range-front semi-arid nested alluvial fan setting (e.g., Bowman, 1978; Colombo, 2005), with at least four main sets of alluvial fans (Matti and Cossette, 2007; Matti et al., 2010; Owen et al., 2014; Kendrick et al., 2015; Fosdick and Blisniuk, 2018).

The exposure along the east and west trench walls indicate consistent lateral continuity of several stratigraphic units with sharp contacts between layers (Figure S1; Castillo et al., 2020). We collected seven and ten samples from the east and west trench walls, respectively. Each sample was from distinct stratigraphic units that did not show evidence of bioturbation or liquefaction (Figures S1, S2). An opaque 5 cm-diameter tube was pushed horizontally into freshly cleaned walls at each sample location and capped immediately to protect from sunlight. We isolated K-feldspar grains of 175–200 μm diameter and density of <2.565 g/cm^3 from the rest of the samples under dim amber LED light conditions at the UCLA Luminescence Laboratory following the procedure of Rhodes (2015) (Supporting Information Text S1).

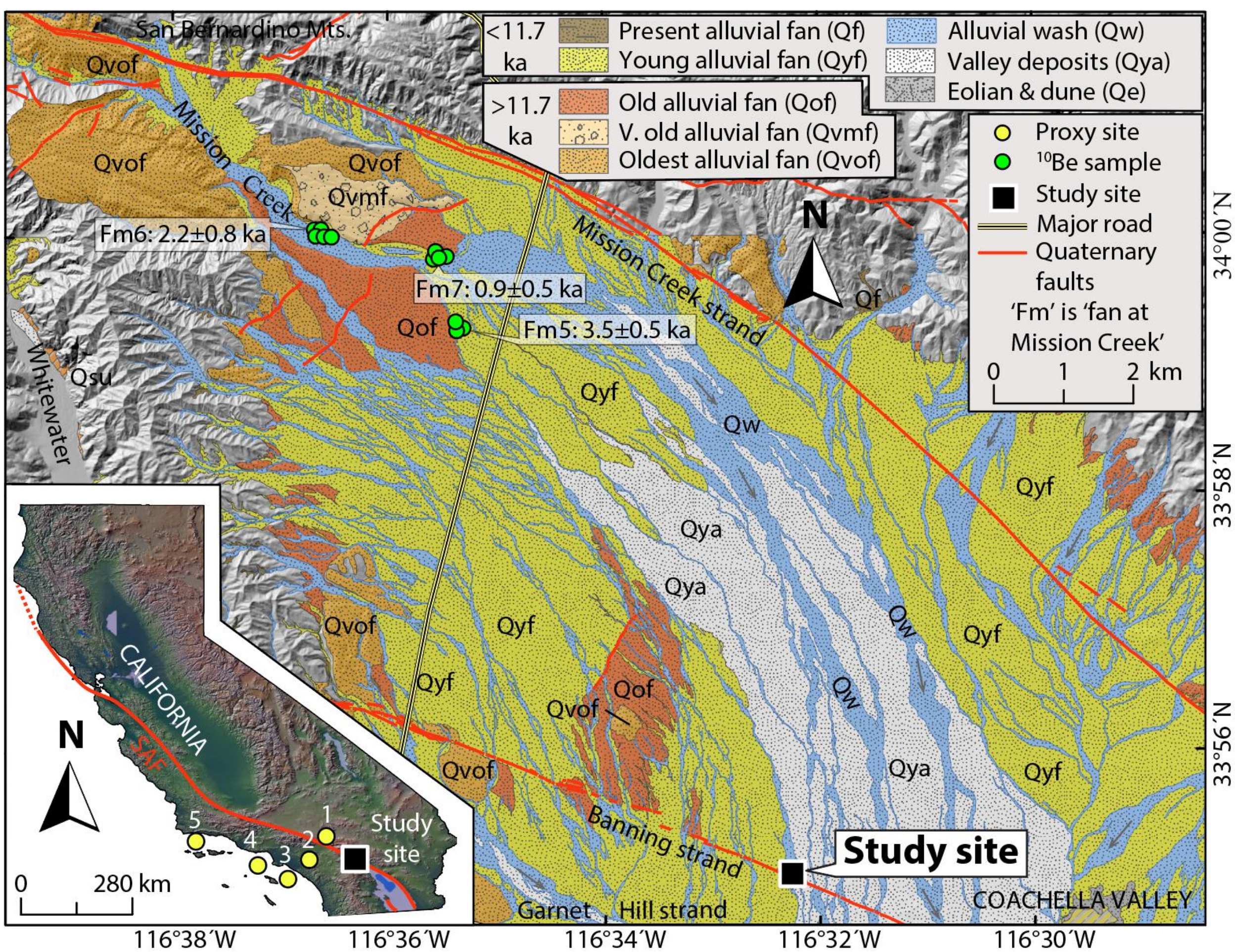

Figure 2. The surficial deposit and fault map of the Mission Creek catchment modified after the Quaternary geological map of southern California (e.g., Lancaster et al., 2012; Kendrick et al., 2015) and the Quaternary Fault and Fold Database of the United States (Hart et al., 2001), respectively. The surficial deposit map is superimposed on a hillshade map generated from the 10-m Shutter Radar Topography Mission (SRTM) Digital Elevation Model (DEM) (USGS, accessed 10/12/2020). Four main sequences of nested alluvial fans (Qvof, Qvmf, Qof, Qyf) at the upper Mission Creek catchment are shown along with ^{10}Be ages of the selected Holocene fans (Owen et al., 2014). Our study site (black square) is located on the Banning strand of the San Andreas Fault (SAF). The inset map in the lower-left shows the location of our study site and the nearby hydroclimatic proxy sites in southern California: 1) Lower Bear Lake (Kirby et al., 2012), 2) Lake Elsinore (Kirby et al., 2010, 2013), 3) Newport submarine fan (Covault et al., 2010), 4) Hueneme submarine fan (Romans et al., 2009), and 5) Santa Barbara Basin (Du et al., 2018)].

2.2 Luminescence Measurements and Age Determination

We carried out the p-IR IRSL measurements using a TL-DA-20 Risø automated reader equipped with a single-grain IR laser (830 nm, at 90% of 150 mW; Bøtter-Jensen et al., 2003). Emissions were detected using an EMI 9235QB photomultiplier tube fitted with a BG3 and BG39 filter combination, allowing transmission around 340–470 nm. A single-grain p-IR IRSL SAR protocol (Buylaert et al., 2009; Rhodes, 2015) was used with a preheat 250°C for 60s and stimulation temperatures of 50°C and 225°C (Text S1).

The total environmental dose rate for each sample was estimated using the *in-situ* measured gamma dose rate (except for sample J1286), and elemental concentrations of U, Th and, K determined using ICP-MS and -OES (Liritzis et al., 2013), estimated internal potassium content of 12.5 ± 0.5 wt.% (Huntley & Baril, 1997), and the contribution from cosmic rays was estimated following Prescott & Hutton (1994). We determined the water content for each sample from their weights before and after drying. In addition, we also tested for the presence of athermal fading (Huntley & Lamothe, 2001) for timescales ranging from ~300 seconds to 7 days (Text; Figure S3A). None of the samples show fading (e.g., Buylaert et al., 2009), and no correction was needed.

The most recent depositional age for each sample was estimated using the minimum age model (MAM; Galbraith et al., 1999) and the central age model (CAM; Galbraith et al., 1999) with overdispersion (OD) of >15% and <15%, respectively (Figure S1a; Castillo et al., 2020). OD is a measure of unexplained equivalent dose variability among grains. We used the DRAC 1.2 online calculator (Durcan et al., 2015) to calculate the most recent depositional ages (Figure S1b) and single-grain ages, assuming a constant radiation dose environment. The analytical uncertainties of single-grain ages due to variable radiation doses and water content were also examined (Figure S3b).

We used the semi-parametric three-parameter finite mixture model (FMM), assuming an OD of 15% to model the ages of single-grain subpopulations (imposing *k* age components). By minimizing the Bayesian Information Criterion (BIC) score from FMM results, one can estimate the most probable number of age components within a population and estimates the age ± 1σ standard error for each component assuming that each component has a Gaussian distribution (hereafter FMM-subpopulations) (Text S1; Figure S4; Galbraith and Green, 1990; Galbraith and Laslett, 1993; Galbraith, 2005; Kreutzer et al., 2012). Since the average relative standard error for single grains in this study is ~10%, we justify using the FMM (c.f. Brandon, 1992). The probability density distribution of single-grain ages for each sample is also shown using the kernel density estimate (KDE) (Figure S4; Kreutzer et al., 2012).

2.3 Depositional History from Single-grain Luminescence Subpopulation Ages

To examine the distribution of single-grain subpopulation ages in all samples collected from multiple stratigraphic units, we calculated individual and composite probability distributions of FMM-subpopulations (Figure S5a). The composite probability density function (PDF) was calculated by summing PDFs of all FMM-subpopulations. However, the potential of recording past subpopulation ages for each sample is restricted to the age ranges older than its last depositional age. Thus, the composite probability for a given age interval was normalized by the total number of samples available for that age interval (Figure S5a). This normalized composite probability shows the relative probability density distribution of depositional ages corrected for sample's availability (hereafter, relative composite probability). For reference, we also showed how (1) the number of samples that can record (henceforth, available samples), (2) the number of samples whose 2σ range overlap (hereafter, overlapping samples), and (3) the fraction of overlapping samples relative to available samples vary with the given age interval (Figure S5c).

In addition, since older ages tend to have larger absolute errors than younger ages (i.e., as age increases, uncertainty increases; e.g., Berger 2010a, 2011; Ivy-Ochs et al., 2007), the probability distribution for older ages often exhibit subdued modal heights (Figure S5a). The opposite is true for young ages with high precision, which often produce overly sharp peaks (Figure S5a). To minimize this bias, we plotted the individual and relative composite probability of FMM-subpopulation ages on a log scale with the corresponding relative probability, calculated based on the Jacobian transformation described in Galbraith (2011) (Text S1; Figures 3a, S5b). The logarithmic scale use of ages and corresponding probability makes it easier to identify multiple modes within the relative composite probability generated from distinctive clusters of FMM-subpopulation ages.

We then identified significant local maxima (modes) in the relative composite probability using the 'findpeaks' function in MATLAB's Signal Processing Toolbox (Text S1). The ages of local maxima identified in both relative composite probability in linear and log scales are identical within 0.1 ka (Figures 3a, S5). Any age clusters identified with <3 overlapping FMM-subpopulations are considered less probable ages. We also did not consider >12 ka FMM-subpopulations since they are comprised of <7 single grains. These are excluded from further analysis (shown with a question mark (?) in Figure 3a; Text S1). We estimated modal age ± 1σ error for each identified local maxima using the Probabilistic Cosmogenic Age Analysis Tool (P-CAAT; Dortch et al., in review). Although P-CAAT is designed to analyze cosmogenic ages, it is useful to separate closely overlapped Gaussian components from the distant ones (i.e., outliers) and estimate the best-fit age ± 1σ for the modeled Gaussian distribution (Text S1; Figure S6).

Finally, the modal ages (Figure 3a) were compared with the selected terrestrial and offshore hydroclimatic proxies (Figure 3b–e) to evaluate whether the modal ages correspond with the periods of certain hydroclimatic conditions.

3 Results

16 of the 17 samples dated using K-feldspar single-grain p-IR $IRSL_{225}$ show OD ranging from ~21–85% (Table S1), yielding much higher OD values than the 15% typical for well-bleached samples from southern California (Rhodes, 2015). Only the sample J1286 is completely bleached with an OD of 9±6% (Table S1), so the CAM was used to date the sample. We used the MAM for the rest of the 16 samples to date the trench's stratigraphic layers for paleoseismic studies (Figure S1b; Castillo et al., 2020). The ages of the stratigraphic units, which are likely the last depositional ages, range between ~8.0 and 0.6 ka. They show a close correspondence with the youngest detrital ^{14}C ages at ± 1σ preserved in those units (Castillo et al., 2020).

We further analyzed the samples using the FMM. Fifty-one FMM-subpopulations were identified from 17 samples, with notable overlap for several time periods (Table S1; Figures 3a, S4). The multiple local maxima shown in KDE plots also closely correspond with those of the FMM populations in each sample (Figure S4).

We identified at least eight prominent local maxima in the past ~12.0 ka from the relative composite probability of the IRSL data (Figure 3a). Seven of the eight local maxima (peak values) estimated using the relative composite probability and the modal ages estimated using P-CAAT are identical at the nearest 0.1 ka (Text S1; Figure 3a). The modal ages that constitute those local maxima are $11.4^{+1.3}_{-1.0}$, 6.9±0.8, 5.5±0.2, 3.6±0.2, 3.0±0.2, 2.4±0.2, 1.6±0.1, and 0.6±0.1 ka (Figures 3a, S5c). Three additional peaks at ~22.3, ~17.2, ~1.2 ka were also identified as local maxima. However, we did not consider these three modal ages further due to limited overlapping Gaussians (<3 subpopulations) or single-grain ages (<7 grains) (Text S1). Additionally, six overlapping FMM-subpopulations cluster around ~9.9 ka (~30%; Figure S5c). However, due to the large errors, they fail to generate any modal distribution distinct from the ~11.4 ka local maxima in the composite probability (Figures 3a, S5a). Similarly, two FMM-subpopulations are observed around ~4 ka, but relative composite probability failed to generate any distinct peak around that time (Figure 3a).

The average interval between significant depositional periods inferred from the modal ages increases with age at the Mission Creek catchment. The average intervals are estimated as ~1.6 (±0.23) ka during the Mid- to Late Holocene (~7–3.6 ka) and ~0.7 (±0.03) ka during the Late Holocene (~3.6–0.6 ka) (Figure S7) based on piecewise linear fits. The depositional periods can also be fitted with an exponential curve giving an appearance of longer intervals between depositional periods back through time (Figure S7).

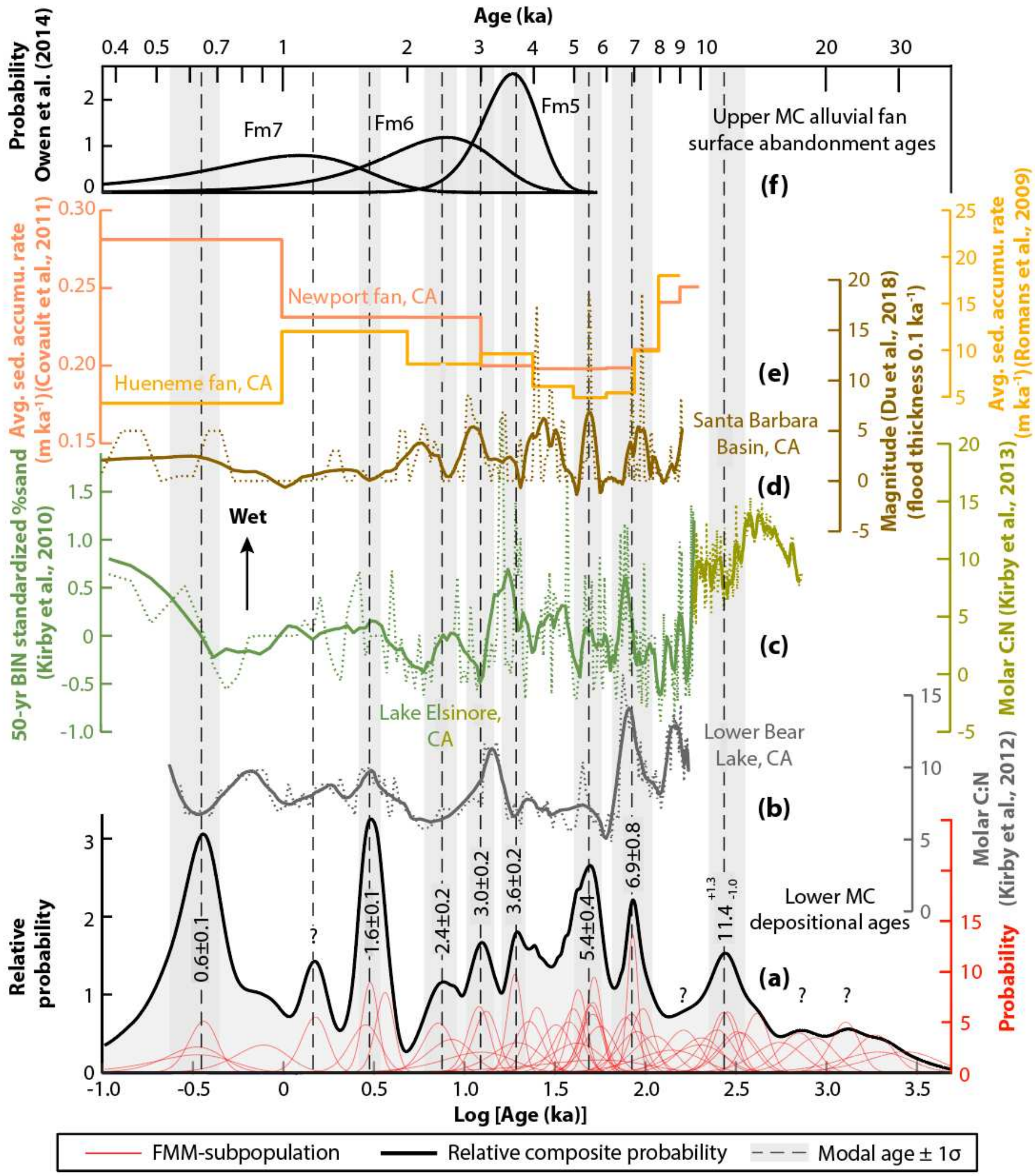

Figure 3. Comparison between the depositional periods, regional hydroclimatic proxies, and upstream alluvial fan surface abandonment ages. (a) The probability distribution of single-grain subpopulation ages was derived using the FMM. The individual subpopulation and their relative composite probability distribution are shown in red and black lines, respectively. The probability is shown for age (ka) in the natural log scale (Galbraith, 2011; see section 2.3).

At least eight prominent Holocene local maxima are identified from the relative composite probability, which likely represents the timing of major depositional periods (modal ages±1σ are shown in gray dash lines and shaded bar, respectively). Question marks indicate less probable local maxima. The hydroclimatic proxies are selected from the nearby terrestrial (b, c) and offshore (d, e) sites. These include (b) Lower Bear Lake (Kirby et al., 2012), (c) Lake Elsinore (yellow-green [19–9 ka] from Kirby et al., 2013 and dark green [9.7–0.2 ka] from Kirby et al., 2010), (d) the Santa Barbara Basin (Du et al., 2018), and (e) the Hueneme and the Newport submarine fans (Romans et al., 2009; Covault et al., 2010). The original and smoothed variations of proxy values are shown in dotted and solid lines, respectively. The ages of all proxies are adjusted to start from AD 2018, consistent with our depositional ages. (f) The probability distribution is based on ^{10}Be surface boulder ages from alluvial fans at the Mission Creek catchment, recalculated from Owen et al. (2014). We used the youngest cluster of each fan (Fm) ages, derived using the P-CAAT model (Text S1).

4 Discussion and Conclusions

We identified at least eight prominent local maxima in the relative composite probability in the last ~12 ka, which likely represents the timing of significant depositional periods in the lower Mission Creek catchment, southern California (Figure 3a). When compared with the regional hydroclimatic proxies (Figure 3b–e), we found a reasonable correspondence between the timing of major depositional periods and the periods of substantially wetter hydroclimatic conditions in southern California over the sub-millennial to millennial timescale (Kirby et al., 2010, 2012, 2013, 2015; Du et al., 2018).

The ~11.4 ka depositional period coincides nicely with the onset of enhanced wetter conditions that prevailed regionally during the Early Holocene (~11.7–7.5 ka). This is shown in the terrestrial molar C:N ratio from Lake Elsinore (Figure 3c) and percent clay from Silver Lake, CA (Kirby et al., 2015). An additional depositional period is possible around ~9.9 ka (Figure 3a) and is highlighted in all the proxies presented in Figure 3 (b–e). However, we failed to generate any peak around ~9.9 ka in our relative composite probability. Further data is required to test this hypothesis. Enhanced summer North American Monsoons (NAM) due to sea surface temperature (SST) change in the Gulf of California (Koehler et al., 2005, Holmgren et al., 2009; Barron et al., 2012) likely triggered high runoff (Kirby et al., 2005, 2007, 2010, 2012; Benson et al., 2002; Bird and Kirby, 2006; Bird et al., 2010; Glover et al., 2017), high soil productivity (Kirby et al., 2015), and increased sediment flux during this time.

Previous studies reported an arid climate in southern California during the Mid-Holocene (~7.5–4.0 ka) with reduced sediment supply, shown by the general decline in molar C:N and weighted-average sediment accumulation rates from Lower Bear Lake and Hueneme and Newport submarine fans, respectively (Figure 3b, e; Romans et al., 2009; Covault et al., 2010; Pigati et al., 2014; Kirby et al., 2012). However, several brief high precipitation/runoff intervals (e.g., ~7.3–6.6, ~5.6–4.7 ka) are recorded in high-resolution terrestrial (e.g., the Lower Bear Lake and the Lake Elsinore cores; Figure 3b, c) and offshore proxies (Santa Barbara Basin ocean cores; Du et al., 2018; Figure 3d), which correspond reasonably well with our depositional periods recorded at ~6.9 and ~5.5 ka (Figure 3a). Substantially wetter intervals are also recorded around ~4.8–4.0 ka in Lake Elsinore and Santa Barbara Basin cores (Figure 3c, d), but interestingly no peaks are identified around that time in the relative composite probability plot (Figure 3a). Although two FMM-subpopulation peaks around ~4 ka are shown (Figure 3a), additional data is required to evaluate any deposition around this time. Frequent enhanced winter storms and winter precipitation regulated by the complex interplay between El Niño and Southern Oscillations (ENSO) and warm Pacific Decadal Oscillations (PDO) likely triggered these brief sediment depositions in an otherwise arid period (Barron et al., 2003; McCabe-Glynn et al., 2013; Wang et al., 2013; Kirby et al., 2015).

Southern California experienced a return to slightly wetter conditions during the Late Holocene (Kirby et al., 2012, 2015) with more frequent ephemeral lakes and periods of increased sediment flux at ~3.7–3.6, ~3.4–3.0, ~2.4, ~2.0–1.4, and 0.9–0.7 ka, as shown in terrestrial lake cores from Lower Bear Lake and Lake Elsinore (Figure 3b, c; Kirby et al., 2010, 2012, 2013) and ocean sediment cores at the Santa Barbara Basin and the Newport deep-sea fan (Figure 3e, f; Covault et al., 2010; Du et al., 2018). Competing climate forcing where insolation forced summer cooling (i.e., weaker NAM) is overridden by ENSO regulated favorable SSTs in the east Pacific (i.e., more winter storms) is likely responsible for this wetter condition during the Late Holocene (Clement et al., 1999). These wetter periods correspond well with the significant deposition at ~3.6, ~3.0, ~2.4, ~1.6, and ~0.6 ka identified in our study site (Figure 3a).

Among the proxies used, the significant Holocene depositional periods inferred from luminescence ages, especially at ~6.9, ~5.4, ~3.0, and ~1.6 ka, shows the best match with the wetter periods determined by molar C:N from the Lower Bear Lake in the San Bernardino Mountains (Figures 3). This proxy is the most proximal to our study site (~52 km). However, the proxies themselves do not show an excellent match except for a few periods due to variable temporal-resolutions and the age models used. This also makes quantification using spectral analysis (e.g., Ólafsdóttir et al., 2016) challenging and statistically a poor fit.

When compared regionally, the inferred Holocene depositional periods also broadly corresponds with the wetter climatic oscillations (±1σ) in the western U.S. identified using rock varnish (e.g., at ~11.8–10.4, ~7.4–6.0, 2.9, 1.5, ~1.2–1.0, ~0.7–0.4 ka; Liu and Broecker, 2007, 2008). Previous studies also showed widespread alluvial fan deposition during wet periods in the American Southwest instead of the arid periods (e.g., Ponti, 1985; Harvey et al., 1999a,b; DeLong and Arnold, 2007; Mahan et al., 2007; Sohn et al., 2007; Liu and Broecker, 2008; Miller et al., 2010; Miller et al., 2010; Owen et al., 2014). Our findings are consistent with this interpretation of significant alluviation in southern California. Interestingly, we also found a broad correspondence between the youngest ^{10}Be age clusters of the alluvial fans (Fm) upstream of the Mission Creek catchment (Owen et al., 2014), likely representing the timing of surface abandonment (e.g., D'Arcy et al., 2019) and the downstream depositional periods (±1σ) at ~3.6, ~2.4, ~1.2 ka from our site (Figures 1, 3f). However, due to considerable uncertainty in ^{10}Be ages (14–56%), we cannot establish direct sediment routing relationships (e.g., Allen and Heller, 2012; Allen et al., 2013; Hoffmann, 2015; Allen, 2017).

While a comprehensive global comparison is beyond this study's scope, similar timing of abrupt climate shifts regulated by changes in the North Atlantic SST during the Holocene is also reported elsewhere in the world (Bond et al., 1997).

We estimated the average intervals of depositional periods to be ~0.7 ka during the Late Holocene and ~1.6 ka during the Mid- to Late Holocene (Figure S7). This apparent increase in the average intervals still exists when we consider the less probable peaks (Figure S7). The changes in period intervals may reflect a shift from Mid-Holocene aridity to Late Holocene pluvial condition (Kirby et al., 2012, 2015). However, these differences could also be the artifacts of preservation bias (e.g., Sadler and Jerolmack, 2015; Miall, 2015) or the limited precision in old ages.

The work presented here is based on simple assumptions and has some limitations. First, we assumed that postdepositional grain mixing due to pedoturbation was limited to none. We collected our samples away from faults and observable liquefactions to minimize the influence of earthquake or ground-shaking induced grain mixing. Additionally, laterally continuous fine sand and silt layers in the trench walls indicate significant pedoturbation likely did not occur, especially below 1 m-depth (Figure S1). However, possible grain mixing due to bioturbation at millennial timescale is widely reported for ~0.3–1.5-m depths (e.g., Lomax et al., 2011; Gliganic et al., 2015, 2016). Hence, the likelihood of undetected grain mixing at shallower depth is possible after the deposition of each stratigraphic unit. Second, because there is no direct way to quantify the dose rate history experienced by a sample, we assume that the past variability in environmental dose rate is within the uncertainty. To evaluate this assumption, we performed a Monte Carlo simulation to estimate the ages based on the range of measured dose rates (i.e., ~4.9 and 6.4 Gy/ka; Text S1) and assumed 5–20% water contents (Figure S3). Our results show that the majority (~76–79%) of the age difference (±1σ) from the ages estimated using constant dose rate and measured water content (used in this study) lies within 20%. These differences are roughly within the 1σ error for most of the Holocene ages. Thus, we argue that this assumption has a negligible impact on our inferred depositional periods. Third, luminescence residuals in feldspar single-grains may introduce age overestimation in some young grains (Li and Li, 2011; Gliganic et al., 2017; Brill et al., 2018). We did not correct for this effect. Fourth, we did not identify the significant periods of erosion. Hence, our estimated depositional periods may be biased by preservation (e.g., Holbrook and Miall, 2020).

Nonetheless, our study shows that luminescence ages of single-grain subpopulations can be used to infer the sediment depositional history beyond the most recent depositional periods. We identified at least eight major Holocene depositional periods at ~11.4, ~6.9, ~5.5, ~3.6, ~3.0, ~2.4, ~1.6, and ~0.6 ka. These depositional periods indicate that climate, especially substantially wetter climate, likely plays the first-order control on sediment deposition over the millennial timescale in southern California (e.g., Akciz and Arrowsmith, 2013). Sediment deposition probably occurred as intermittent pulses with an average interval of ~0.7–1.6 ka controlled by regional and local hydroclimatic variations (e.g., Burt and Allison, 2010; Allen, 2017; Caracciolo et al., 2020). Our work therefore has important implications for tectonic or paleoclimatic studies that rely on stratigraphic completeness, especially in terrestrial settings (e.g., Washburn et al., 2003; Béon et al., 2018), and must be considered when interpreting the fault slip rates or paleoclimatic events in southern California.

Acknowledgments

We thank Marina Argueta and Norma Contreras for sample preparation. Thanks to Justin Higa for constructive comments to improve the manuscript, John Rogers for granting access to the trench site, and Alan Pace from Petra Geosciences to accommodate this study. We thank the supports from the USGS EHP Awards G18A00040, G18A00041, G20AP00044, and the NSF EAR-1728145. The data used in this study are being achieved on PANGAEA, and the DOI will be made available soon. However, we temporarily uploaded a copy of the data as Supporting Information for review purposes.

References

Akçiz, S. O., & Arrowsmith, J. R. (2013). New views on the evolution of the San Andreas fault zone in central California and the Carrizo Plain. Field Guide 32, *Geological Society of America, 1–12.*

Allen, G. H., Barnes, J. B., Pavelsky, T. M., & Kirby, E. (2013). Lithologic and tectonic controls on bedrock channel form at the northwest Himalayan front. Journal of Geophysical Research: Earth Surface, 118(3), 1806–1825. https://doi.org/10.1002/jgrf.20113

Allen, P. A. & Heller, P. L. (2012). Dispersal and preservation of tectonically generated alluvial gravels in sedimentary basins. *In:* Busby, C. & Azor, A. (eds) *Tectonics of Sedimentary Basins: Recent Advances*. Wiley–Blackwell, Chichester, 111–130.

Allen, P.A. (2017). Sediment Routing Systems. The Fate of Sediments from Source to Sink. Cambridge University Press, Cambridge. https://doi.org/10.1017/9781316135754.

Armitage, J. J., Duller, R. A., Whittaker, A. C., & Allen, P. A. (2011). Transformation of tectonic and climatic signals from source to sedimentary archive. Nature Geoscience, 4(4), 231–235. https://doi.org/10.1038/ngeo1087

Armitage, J. J., Dunkley Jones, T., Duller, R. A., Whittaker, A. C., & Allen, P. A. (2013). Temporal buffering of climate-driven sediment flux cycles by transient catchment response. Earth and Planetary Science Letters, 369–370, 200–210. https://doi.org/10.1016/j.epsl.2013.03.020

Barron, J. A., Heusser, L., Herbert, T., & Lyle, M. (2003). High-resolution climatic evolution of coastal northern California during the past 16,000 years. Paleoceanography, 18(1). https://doi.org/10.1029/2002PA000768

Barron, J. A., Metcalfe, S. E., & Addison, J. A. (2012). Response of the North American monsoon to regional changes in ocean surface temperature. Paleoceanography, 27(3). https://doi.org/10.1029/2011PA002235

Benson, S. R., Croll, D. A., Marinovic, B. B., Chavez, F. P., & Harvey, J. T. (2002). Changes in the cetacean assemblage of a coastal upwelling ecosystem during El Niño 1997-98 and La Niña 1999. Progress in Oceanography, 54(1–4), 279–291. https://doi.org/10.1016/S0079-6611(02)00054-X

Berger, G. (2010). An alternate form of probability-distribution plots for DE values. Ancient TL, 28(1), 11–21.

Berger, G. W. (2011). Response to Galbraith. *Ancient TL, 29*, 48–50.

Bird, B. W., & Kirby, M. E. (2006). An alpine lacustrine record of early Holocene North American Monsoon dynamics from Dry Lake, southern California (USA). Journal of Paleolimnology, 35(1), 179–192. https://doi.org/10.1007/s10933-005-8514-3

Bird, B. W., Kirby, M. E., Howat, I. M., & Tulaczyk, S. (2010). Geophysical evidence for Holocene lake-level change in southern California (Dry Lake). Boreas, 39(1), 131–144. https://doi.org/10.1111/j.1502-3885.2009.00114.x

Bond, G., Showers, W., Cheseby, M., Lotti, R., Almasi, P., DeMenocal, P., Priore, P., Cullen, H., Hajdas, I., & Bonani, G. (1997). A pervasive millennial-scale cycle in North Atlantic Holocene and glacial climates. Science, 278(5341), 1257–1266. https://doi.org/10.1126/science.278.5341.1257

Bøtter-Jensen, L., McKeever, S. W. S., & Wintle, A. G. (2003). Optically Stimulated Luminescence Dosimetry. Optically Stimulated Luminescence Dosimetry, 1–355. https://doi.org/10.1016/B978-0-444-50684-9.X5077-6

Bowman, D. (1978). Determination of intersection points within a telescopic alluvial fan complex. *Earth Surface Processes, 3*, 265–276.

Brandon, Mark T. (1992). Decomposition of fission-track grain-age distributions. American Journal of Science, 292, 535–564.

Brill, D., Reimann, T., Wallinga, J., May, S. M., Engel, M., Riedesel, S., & Brückner, H. (2018). Testing the accuracy of feldspar single grains to date late Holocene cyclone and tsunami deposits. Quaternary Geochronology, 48(August), 91–103. https://doi.org/10.1016/j.quageo.2018.09.001

Brown, N. D. (2020). Which geomorphic processes can be informed by luminescence measurements? Geomorphology, 367, 107296. https://doi.org/10.1016/j.geomorph.2020.107296

Bull, W. B. (1977). The alluvial-fan environment. *Prog. Phys. Geogr. 1*, 222–270.

Bull, W. B. (1991). Geomorphic Responses to Climate Change. Oxford University Press, New York.

Bull, W. B. (2000). Correlation of fluvial aggradation events to times of global climate change. *In: Noller, J. S., Sowers, J. M., Lettis, W. R. (eds.), Quaternary Geochronology: Methods and Applications.* American Geophysical Union, Washington, D.C., pp. 456–464.

Bull, W. B. (2007). Tectonic Geomorphology of Mountains: a New Approach to Paleoseismology. Blackwell Publishing, p. 328.

Burt, T. P., & Allison, R. J. (2010). Sediment cascades. *In: Burt, T. P., Allison, R. J. (eds.), Sediment Cascades in the Environment: An Integrated Approach.* John Wiley and Sons, pp. 1–15.

Buylaert, J. P., Murray, A. S., Thomsen, K. J., & Jain, M. (2009). Testing the potential of an elevated temperature IRSL signal from K-feldspar. Radiation Measurements, 44(5–6), 560–565. https://doi.org/10.1016/j.radmeas.2009.02.007

Caracciolo, L., Chew, D., & Andò, S. (2020). Sediment Generation and Sediment Routing Systems. Earth-Science Reviews, 207(June). https://doi.org/10.1016/j.earscirev.2020.103221

Castillo, B., McGill1, S. F., Scharer, K. M., Yule, J. D., McPhillips, D., McNeil, J., Saha, S., Brown, N. D. & Moon, S. (2020). Prehistoric Earthquakes on the Banning Strand of the San Andreas Fault, North Palm Springs, California. Geosphere (in pre-print).

Clement, A. C., Seager, R., & Cane, M. A. (1999). Orbital controls on the El Nino/Southern Oscillation and the tropical climate. Paleoceanography, 14(4), 441–456. https://doi.org/10.1029/1999PA900013

Colarossi, D., Duller, G. A. T., Roberts, H. M., Tooth, S., & Lyons, R. (2015). Quaternary Geochronology Comparison of paired quartz OSL and feldspar post-IR IRSL dose distributions in poorly bleached fl uvial sediments from South Africa. Quaternary Geochronology, 30, 233–238. https://doi.org/10.1016/j.quageo.2015.02.015

Covault, J. A., Romans, B. W., Fildani, A., McGann, M., & Graham, S. A. (2010). Rapid climatic signal propagation from source to sink in a southern California sediment-routing system. Journal of Geology, 118(3), 247–259. https://doi.org/10.1086/651539

D'arcy, M. K., Schildgen, T. F., Turowski, J. M., & Dinezio, P. (2019). Inferring the timing of abandonment of aggraded alluvial surfaces dated with cosmogenic nuclides. Earth Surface Dynamics, 7(3), 755–771. https://doi.org/10.5194/esurf-7-755-2019

DeLong, S. B., & Arnold, L. J. (2007). Dating alluvial deposits with optically stimulated luminescence, AMS 14C and cosmogenic techniques, western Transverse Ranges, California, USA. Quaternary Geochronology, 2(1–4), 129–136. https://doi.org/10.1016/j.quageo.2006.03.012

Dortch, J. M., Tomkins, M. D., Saha, S., Murari, M. K., Schoenbohm, L. M., & Curl, D. (in review). Probabilistic Cosmogenic Age Analysis Tool (P-CAAT), a tool for the ages. http://kgs.uky.edu/anorthite/PCAAT/.

Du, X., Hendy, I., & Schimmelmann, A. (2018). A 9000-year flood history for Southern California: A revised stratigraphy of varved sediments in Santa Barbara Basin. Marine Geology, 397(May 2017), 29–42. https://doi.org/10.1016/j.margeo.2017.11.014

Duller, G. A. T. (2004). Luminescence dating of Quaternary sediments: Recent advances. Journal of Quaternary Science, 19(2), 183–192. https://doi.org/10.1002/jqs.809

Durcan, J. A., King, G. E., & Duller, G. A. T. (2015). Quaternary Geochronology DRAC : Dose Rate and Age Calculator for trapped charge dating. Quaternary Geochronology, 28, 54–61. https://doi.org/10.1016/j.quageo.2015.03.012

Fosdick, J. C., & Blisniuk, K. (2018). Sedimentary signals of recent faulting along an old strand of the San Andreas Fault, USA. Scientific Reports, 8(1), 1–10. https://doi.org/10.1038/s41598-018-30622-3

Fuchs, M., & Owen, L. A. (2008). Luminescence dating of glacial and associated sediments: review, recommendations and future directions. Boreas, 37(4), 636–659. https://doi.org/10.1111/j.1502-3885.2008.00052.x

Galbraith, R. (2011) Some comments arising from Berger (2010). *Ancient TL 29*, 41–47.

Galbraith, R. F. (2005). Statistics for Fission Track Analysis. Chapman and Hall/CRC, London.

Galbraith, R. F., & Green, P. F. (1990). Estimating the component ages in a finite mixture. International Journal of Radiation Applications and Instrumentation. Part, 17(3), 197–206. https://doi.org/10.1016/1359-0189(90)90035-V

Galbraith, R. F., & Laslett, G. M. (1993). Statistical models for mixed fission track ages. International Journal of Radiation Applications and Instrumentation. Part, 21(4), 459–470. https://doi.org/10.1016/1359-0189(93)90185-C

Galbraith, R. F., Roberts, R. G., Laslett, G. M., Yoshida, H., & Olley, J. M. (1999). Optical dating of single and multiple grains of quartz from Jinmium rock shelter, northern Australia: part i, experimental design and statistical models*. Archaeometry, 2(February), 339–364.

Geologia, F. De, & Barcelona, U. De. (2019). Quaternary telescopic-like alluvial fans, Andean Ranges, Argentina, 69–84.

Gliganic, L. A., Cohen, T. J., Meyer, M., & Molenaar, A. (2017). Variations in luminescence properties of quartz and feldspar from modern fluvial sediments in three rivers. Quaternary Geochronology, 41, 70–82. https://doi.org/10.1016/j.quageo.2017.06.005

Gliganic, L. A., May, J. H., & Cohen, T. J. (2015). All mixed up: Using single-grain equivalent dose distributions to identify phases of pedogenic mixing on a dryland alluvial fan. Quaternary International, 362(1), 23–33. https://doi.org/10.1016/j.quaint.2014.07.040

Gliganic, Luke Andrew, Cohen, T. J., Slack, M., & Feathers, J. K. (2016). Sediment mixing in aeolian sandsheets identified and quantified using single-grain optically stimulated luminescence. Quaternary Geochronology, 32, 53–66. https://doi.org/10.1016/j.quageo.2015.12.006

Glover, K. C., MacDonald, G. M., Kirby, M. E., Rhodes, E. J., Stevens, L., Silveira, E., Whitaker, A., & Lydon, S. (2017). Evidence for orbital and North Atlantic climate forcing in alpine Southern California between 125 and 10 ka from multi-proxy analyses of Baldwin Lake. Quaternary Science Reviews, 167, 47–62. https://doi.org/10.1016/j.quascirev.2017.04.028

Gray, H. J., Jain, M., Sawakuchi, A. O., Mahan, S. A., & Tucker, G. E. (2019). Luminescence as a Sediment Tracer and Provenance Tool. Reviews of Geophysics, 57(3), 987–1017. https://doi.org/10.1029/2019RG000646

Gray, H. J., Tucker, G. E., Mahan, S. A., & Al, G. E. T. (2018). Application of a Luminescence-Based Sediment Transport Model, 6071–6080. https://doi.org/10.1029/2018GL078210

Guérin, G., Mercier, N., Nathan, R., Adamiec, G., & Lefrais, Y. (2012). On the use of the infinite matrix assumption and associated concepts: A critical review. Radiation Measurements, 47(9), 778–785. https://doi.org/10.1016/j.radmeas.2012.04.004

Hart, E. W., & Bryant, W. A., compilers. (2001). Fault number 30a, Maacama fault zone, northern section, in Quaternary fault and fold database of the United States: U.S. Geological Survey website, https://earthquakes.usgs.gov/hazards/qfaults, accessed 10/12/2020 10:50 AM.

Harvey, A. M., Silva, P. G., Mather, A. E., Goy, J. L., Stokes, M., & Zazo, C. (1999). The impact of Quaternary sea-level and climatic change on coastal alluvial fans in the Cabo de Gata ranges, southeast Spain. Geomorphology, 28(1–2), 1–22. https://doi.org/10.1016/S0169-555X(98)00100-7

Harvey, A. M., Wigand, P. E., & Wells, S. G. (1999). Response of alluvial fan systems to the late Pleistocene to Holocene climatic transition: Contrasts between the margins of pluvial Lakes Lahontan and Mojave, Nevada and California, USA. Catena, 36(4), 255–281. https://doi.org/10.1016/S0341-8162(99)00049-1

Hoffmann, T. (2015). Sediment residence time and connectivity in non-equilibrium and transient geomorphic systems. Earth-Science Reviews, 150, 609–627. https://doi.org/10.1016/j.earscirev.2015.07.008

Holbrook, J. M., & Miall, A. D. (2020). Time in the Rock: A field guide to interpreting past events and processes from siliciclastic stratigraphy. Earth-Science Reviews, 203, 103121. https://doi.org/10.1016/j.earscirev.2020.103121

Holmgren, C. A., Betancourt, J. L., & Rylander, K. A. (2010). A long-term vegetation history of the Mojave–Colorado Desert ecotone at Joshua Tree National Park. *Journal of Quaternary Science 25(2)*, 222–236.

Huntley, D. J., & Lamothe, M. (2001). Ubiquity of anomalous fading in K-feldspars and the measurement and correction for it in optical dating, 1106, 1093–1106. https://doi.org/10.1139/cjes-38-7-1093

Huntley, D., & Baril, M. (1997). The K content of the K-feldspars being measured in optical dating or in thermoluminescence dating. Ancient TL, 15(1), 11–13.

Inman, D. L., & Jenkins, S. A. (1999). Climate change and the episodicity of sediment flux of small California Rivers. Journal of Geology, 107(3), 251–270. https://doi.org/10.1086/314346

Ivy-Ochs, S., Kerschner, H., & Schlüchter, C. (2007). Cosmogenic nuclides and the dating of Lateglacial and Early Holocene glacier variations: The Alpine perspective. Quaternary International, 164–165, 53–63. https://doi.org/10.1016/j.quaint.2006.12.008

Jerolmack, D. J., & Paola, C. (2010). Shredding of environmental signals by sediment transport. Geophysical Research Letters, 37(19), 1–5. https://doi.org/10.1029/2010GL044638

Kendrick, K. J., Matti, J. C., & Mahan, S. A. (2015). Late quaternary slip history of the Mill Creek strand of the San Andreas fault in San Gorgonio Pass, southern California: The role of a subsidiary left-lateral fault in strand switching. Bulletin of the Geological Society of America, 127(5–6), 825–849. https://doi.org/10.1130/B31101.1

Kirby, E., Harkins, N., Wang, E., Shi, X., Fan, C., & Burbank, D. (2007). Slip rate gradients along the eastern Kunlun fault. Tectonics, 26(2), 1–16. https://doi.org/10.1029/2006TC002033

Kirby, M. E., Lund, S. P., Patterson, W. P., Anderson, M. A., Bird, B. W., Ivanovici, L., Monarrez, P., & Nielsen, S. (2010). A Holocene record of Pacific Decadal Oscillation (PDO)-related hydrologic variability in Southern California (Lake Elsinore, CA). Journal of Paleolimnology, 44(3), 819–839. https://doi.org/10.1007/s10933-010-9454-0

Kirby, Matthew E., Feakins, S. J., Bonuso, N., Fantozzi, J. M., & Hiner, C. A. (2013). Latest Pleistocene to Holocene hydroclimates from Lake Elsinore, California. Quaternary Science Reviews, 76, 1–15. https://doi.org/10.1016/j.quascirev.2013.05.023

Kirby, Matthew E., Feakins, S. J., Hiner, C. A., Fantozzi, J., Zimmerman, S. R. H., Dingemans, T., & Mensing, S. A. (2014). Tropical Pacific forcing of Late-Holocene hydrologic variability in the coastal southwest United States. Quaternary Science Reviews, 102, 27–38. https://doi.org/10.1016/j.quascirev.2014.08.005

Kirby, Matthew E., Knell, E. J., Anderson, W. T., Lachniet, M. S., Palermo, J., Eeg, H., Lucero, R., Murrieta, R., Arevalo, A., & Silveira, E., Hiner, C. A. (2015). Evidence for insolation and Pacific forcing of late glacial through Holocene climate in the Central Mojave Desert (Silver Lake, CA). Quaternary Research (United States), 84(2), 174–186. https://doi.org/10.1016/j.yqres.2015.07.003

Kirby, Matthew E., Lund, S. P., & Poulsen, C. J. (2005). Hydrologic variability and the onset of modern El Niño-Southern Oscillation: A 19 250-year record from Lake Elsinore, southern California. Journal of Quaternary Science, 20(3), 239–254. https://doi.org/10.1002/jqs.906

Kirby, Matthew E., Zimmerman, S. R. H., Patterson, W. P., & Rivera, J. J. (2012). A 9170-year record of decadal-to-multi-centennial scale pluvial episodes from the coastal Southwest United States: A role for atmospheric rivers? Quaternary Science Reviews, 46, 57–65. https://doi.org/10.1016/j.quascirev.2012.05.008

Koehler, P. A., Anderson, R. S., & Spaulding, W. G. (2005). Development of vegetation in the Central Mojave Desert of California during the late Quaternary. Palaeogeography, Palaeoclimatology, Palaeoecology, 215(3–4), 297–311. https://doi.org/10.1016/j.palaeo.2004.09.010

Kreutzer, S., Schmidt, C., Fuchs, M. C., Dietze, M., & Fuchs, M. (2012). Introducing an R package for luminescence dating analysis, 30(1), 1–8.

Lancaster, J.T., Hayhurst, C.A., and Bedrossian, T.L., compilers, 2012, Preliminary Geologic Map of Quaternary Superficial Deposits in Southern California Palm Springs 30′ _× 60′ _Quadrangle: California Geological Survey Special Report 217, Plate 24, scale 1:100,000. https://www.conservation.ca.gov/cgs/publications/sr217

Le Béon, M., Tseng, Y. C., Klinger, Y., Elias, A., Kunz, A., Sursock, A., Daëron, M., Tapponnier, P., & Jomaa, R. (2018). High-resolution stratigraphy and multiple luminescence dating techniques to reveal the paleoseismic history of the central Dead Sea fault (Yammouneh fault, Lebanon). Tectonophysics, 738–739(April), 1–15. https://doi.org/10.1016/j.tecto.2018.04.009

Li, B., & Li, S. (2011). Quaternary Geochronology Luminescence dating of K-feldspar from sediments : A protocol without anomalous fading correction, 6, 468–479. https://doi.org/10.1016/j.quageo.2011.05.001

Lian, O. B., & Roberts, R. G. (2006). Dating the Quaternary: progress in luminescence dating of sediments. Quaternary Science Reviews, 25(19–20), 2449–2468. https://doi.org/10.1016/j.quascirev.2005.11.013

Liritzis, I. (2013). Luminescence Dating in Archaeology, Anthropology, and Geoarchaeology: An Overview (SpringerBriefs in Earth System Sciences). Retrieved from https://www.amazon.com/Luminescence-Dating-Archaeology-Anthropology-Geoarchaeology/dp/3319001698

Liu, T., & Broecker, W. S. (2007). Holocene rock varnish microstratigraphy and its chronometric application in the drylands of western USA. Geomorphology, 84(1–2), 1–21. https://doi.org/10.1016/j.geomorph.2006.06.008

Liu, T., & Broecker, W. S. (2008). Rock varnish evidence for latest Pleistocene millennial-scale wet events in the drylands of western United States. Geology, 36(5), 403–406. https://doi.org/10.1130/G24573A.1

Lomax, J., Hilgers, A., & Radtke, U. (2011). Palaeoenvironmental change recorded in the palaeodunefields of the western Murray Basin, South Australia - New data from single grain OSL-dating. Quaternary Science Reviews, 30(5–6), 723–736. https://doi.org/10.1016/j.quascirev.2010.12.015

Mccabe-Glynn, S., Johnson, K. R., Strong, C., Berkelhammer, M., Sinha, A., Cheng, H., & Edwards, R. L. (2013). Variable North Pacific influence on drought in southwestern North America since AD 854. Nature Geoscience, 6(8), 617–621. https://doi.org/10.1038/ngeo1862

Miall, A. D. (2015). Updating uniformitarianism: stratigraphy as just a set of 'frozen accidents.' *In: Smith, D. G., Bailey, R. J., Burgess, P. M., Fraser, A. J. (eds.), Strata and Time:*

Probing the Gaps in Our Understanding. Geological Society, London, Special Publications, pp. 404.

Miller, S. R., Fitzgerald, P. G., & Baldwin, S. L. (2010). Cenozoic range-front faulting and development of the Transantarctic Mountains near Cape Surprise, Antarctica: Thermochronologic and geomorphologic constraints. Tectonics, 29(1), 1–21. https://doi.org/10.1029/2009TC002457

Milliman, J. D., & Kao, S. J. (2005). Hyperpycnal discharge of fluvial sediment to the ocean: Impact of super-typhoon herb (1996) on Taiwanese rivers. Journal of Geology, 113(5), 503–516. https://doi.org/10.1086/431906

Ólafsdóttir, K. B., Schulz, M., & Mudelsee, M. (2016). REDFIT-X: Cross-spectral analysis of unevenly spaced paleoclimate time series. Computers and Geosciences, 91, 11–18. https://doi.org/10.1016/j.cageo.2016.03.001

Owen, L. A., Clemmens, S. J., Finkel, R. C., & Gray, H. (2014). Late Quaternary alluvial fans at the eastern end of the San Bernardino Mountains, Southern California. Quaternary Science Reviews, 87, 114–134. https://doi.org/10.1016/j.quascirev.2014.01.003

Pigati, J. S., Rech, J. A., Quade, J., & Bright, J. (2014). Desert wetlands in the geologic record. Earth-Science Reviews, 132, 67–81. https://doi.org/10.1016/j.earscirev.2014.02.001

Ponti, D. J. (1985). The quaternary alluvial sequence of the antelope valley, California. Special Paper of the Geological Society of America, 203, 79–96. https://doi.org/10.1130/SPE203-p79

Prescott, J. R., & Hutton, J. T. (1994). Cosmic ray contributions to dose rates for luminescence and ESR dating: Large depths and long-term time variations. Radiation Measurements, 23(2–3), 497–500. https://doi.org/10.1016/1350-4487(94)90086-8

Reimann, T., Thomsen, K. J., Jain, M., Murray, A. S., & Frechen, M. (2012). Single-grain dating of young sediments using the pIRIR signal from feldspar. Quaternary Geochronology, 11, 28–41. https://doi.org/10.1016/j.quageo.2012.04.016

Rhodes, E. J. (2011). Optically Stimulated Luminescence Dating of Sediments over the Past 200,000 Years. https://doi.org/10.1146/annurev-earth-040610-133425

Rhodes, E. J. (2015). Dating sediments using potassium feldspar single-grain IRSL: Initial methodological considerations. Quaternary International, 362, 14–22. https://doi.org/10.1016/j.quaint.2014.12.012

Romans, B. W., Castelltort, S., Covault, J. A., Fildani, A., & Walsh, J. P. (2016). Environmental signal propagation in sedimentary systems across timescales. Earth-Science Reviews, 153, 7–29. https://doi.org/10.1016/j.earscirev.2015.07.012

Romans, B. W., Normark, W. R., McGann, M. M., Covault, J. A., & Graham, S. A. (2009). Coarse-grained sediment delivery and distribution in the Holocene Santa Monica Basin, California: Implications for evaluating source-to-sink flux at millennial time scales. Bulletin of the Geological Society of America, 121(9–10), 1394–1408. https://doi.org/10.1130/B26393.1

Sadler, P. M., & Jerolmack, D. J. (2015). Scaling laws for aggradation, denudation and progradation rates: The case for timescale invariance at sediment sources and sinks. Geological Society Special Publication, 404, 69–88. https://doi.org/10.1144/SP404.7

Smedley, R. K., Duller, G. A. T., & Roberts, H. M. (2015). Bleaching of the post-IR IRSL signal from individual grains of K-feldspar: Implications for single-grain dating. Radiation Measurements, 79, 33–42. https://doi.org/10.1016/j.radmeas.2015.06.003

Sohn, M. F., Mahan, S. A., Knott, J. R., & Bowman, D. D. (2007). Luminescence ages for alluvial-fan deposits in Southern Death Valley: Implications for climate-driven sedimentation along a tectonically active mountain front. Quaternary International, 166(1), 49–60. https://doi.org/10.1016/j.quaint.2007.01.002

Spelz, R. M., Fletcher, J. M., Owen, L. A., & Caffee, M. W. (2008). Quaternary alluvial-fan development, climate and morphologic dating of fault scarps in Laguna Salada, Baja California, Mexico. Geomorphology, 102(3–4), 578–594. https://doi.org/10.1016/j.geomorph.2008.06.001

Toby, S. C., Duller, R. A., De Angelis, S., & Straub, K. M. (2019). A Stratigraphic Framework for the Preservation and Shredding of Environmental Signals. Geophysical Research Letters, 46(11), 5837–5845. https://doi.org/10.1029/2019GL082555

Wallinga, J. (2002). Optically stimulated luminescence dating of fluvial deposits: A review. Boreas, 31(4), 303–322. https://doi.org/10.1080/030094802320942536

Wang, F., Liu, Z., & Notaro, M. (2013). Extracting the dominant SST modes impacting North America's observed climate. Journal of Climate, 26(15), 5434–5452. https://doi.org/10.1175/JCLI-D-12-00583.1

Washburn, Z., Arrowsmith, J. R., Dupont-Nivet, G., Wang, X. F., Zhang, Y. Q., & Chen, Z. (2003). Paleoseismology of the Xorxol Segment of the Central Altyn Tagh Fault, Xinjiang, China. Annals of Geophysics, 46(5), 1015–1034. https://doi.org/10.4401/ag-3443

Wells, S. G., McFadden, L. D., & Dohrenwend, J. C. (1987). Influence of late Quaternary climatic changes on geomorphic and pedogenic processes on a desert piedmont, Eastern

Mojave Desert, California. Quaternary Research, 27(2), 130–146. https://doi.org/10.1016/0033-5894(87)90072-X

Wells, S. G., McFadden, L. D., & Harden, J. (1990). Preliminary results of age estimations and regional correlations of Quaternary alluvial fans within the Mojave Desert in southern California. *In: Reynolds, R. E., Wells, S. G., Brady, R. H. (eds.), At the End of the Mojave— Quaternary Studies in the Eastern Mojave Desert. San Bernardino County Museum Association, Redlands, California*, pp. 45–54.

Wintle, A. G. (1997). Luminescence dating: Laboratory procedures and protocols. Radiation Measurements, 27(5–6), 769–817. https://doi.org/10.1016/S1350-4487(97)00220-5

References From the Supporting Information

Balco, G., Stone, J. O., Lifton, N. A., & Dunai, T. J. (2008). A complete and easily accessible means of calculating surface exposure ages or erosion rates from 10Be and 26Al measurements. Quaternary Geochronology, 3(3), 174–195. https://doi.org/10.1016/j.quageo.2007.12.001

Brennan, B. J., Lyons, R. G., & Phillips, S. W. (1991). Attenuation of alpha particle track dose for spherical grains. International Journal of Radiation Applications and Instrumentation. Part, 18(1–2), 249–253. https://doi.org/10.1016/1359-0189(91)90119-3

Buylaert, J. P., Murray, A. S., Thomsen, K. J., & Jain, M. (2009). Testing the potential of an elevated temperature IRSL signal from K-feldspar. Radiation Measurements, 44(5–6), 560–565. https://doi.org/10.1016/j.radmeas.2009.02.007

Castillo, B., McGill1, S. F., Scharer, K. M., Yule, J. D., McPhillips, D., McNeil, J., Saha, S., Brown, N. D. & Moon, S. (2020). Prehistoric Earthquakes on the Banning Strand of the San Andreas Fault, North Palm Springs, California. Geosphere (in pre-print).

D'arcy, M. K., Schildgen, T. F., Turowski, J. M., & Dinezio, P. (2019). Inferring the timing of abandonment of aggraded alluvial surfaces dated with cosmogenic nuclides. Earth Surface Dynamics, 7(3), 755–771. https://doi.org/10.5194/esurf-7-755-2019

Dortch, J. M., Tomkins, M. D., Saha, S., Murari, M. K., Schoenbohm, L. M., & Curl, D. (in review). Probabilistic Cosmogenic Age Analysis Tool (P-CAAT), a tool for the ages. http://kgs.uky.edu/anorthite/PCAAT/)

Durcan, J. A., King, G. E., & Duller, G. A. T. (2015). Quaternary Geochronology DRAC : Dose Rate and Age Calculator for trapped charge dating. Quaternary Geochronology, 28, 54–61. https://doi.org/10.1016/j.quageo.2015.03.012

Gabriel Marsh (2021). LOESS regression smoothing (https://www.mathworks.com/matlabcentral/fileexchange/55407-loess-regression-smoothing), MATLAB Central File Exchange. Retrieved January 30, 2021.

Galbraith, R. (2011) Some comments arising from Berger (2010). Ancient TL 29, 41–47.

Galbraith, R. F., Roberts, R. G., Laslett, G. M., Yoshida, H., & Olley, J. M. (1999). Optical dating of single and multiple grains of quartz from Jinmium rock shelter, northern Australia: part i, experimental design and statistical models*. Archaeometry, 2(February), 339–364.

Guerin, G., Mercier, N., Nathan, R., Adamiec, C., & Lefrais, Y. (2012). On the use of the infinite matrix assumption and associated concepts: a critical review. Radiat. Meas. 47, 778–785. https://doi.org/10.1016/j.radmeas.2012.04.004

Huntley, D. J., & Lamothe, M. (2001). Ubiquity of anomalous fading in K-feldspars and the measurement and correction for it in optical dating, 1106, 1093–1106. https://doi.org/10.1139/cjes-38-7-1093

Huntley, D., & Baril, M. (1997). The K content of the K-feldspars being measured in optical dating or in thermoluminescence dating. Ancient TL, 15(1), 11–13.

Kreutzer, S., Schmidt, C., Fuchs, M. C., Dietze, M., & Fuchs, M. (2012). Introducing an R package for luminescence dating analysis, 30(1), 1–8.

Liritzis, I. (2013). Luminescence Dating in Archaeology, Anthropology, and Geoarchaeology: An Overview (SpringerBriefs in Earth System Sciences). Retrieved from https://www.amazon.com/Luminescence-Dating-Archaeology-Anthropology-Geoarchaeology/dp/3319001698

Liritzis, I. (2013). Luminescence Dating in Archaeology, Anthropology, and Geoarchaeology: An Overview (SpringerBriefs in Earth System Sciences). Retrieved from https://www.amazon.com/Luminescence-Dating-Archaeology-Anthropology-Geoarchaeology/dp/3319001698

McGuire, C., & Rhodes, E. J. (2015). Downstream MET-IRSL single-grain distributions in the Mojave River, southern California: Testing assumptions of a virtual velocity model. Quaternary Geochronology, 30, 239–244. https://doi.org/10.1016/j.quageo.2015.02.004

Murray, A. S., & Wintle, A. G. (2000). Luminescence dating of quartz using an improved single-aliquot regenerative-dose protocol. Radiation Measurements, 32(1), 57–73. https://doi.org/10.1016/S1350-4487(99)00253-X

Owen, L. A., Clemmens, S. J., Finkel, R. C., & Gray, H. (2014). Late Quaternary alluvial fans at the eastern end of the San Bernardino Mountains, Southern California. Quaternary Science Reviews, 87, 114–134. https://doi.org/10.1016/j.quascirev.2014.01.003

Prescott, J. R., & Hutton, J. T. (1994). Cosmic ray contributions to dose rates for luminescence and ESR dating: Large depths and long-term time variations. Radiation Measurements, 23(2–3), 497–500. https://doi.org/10.1016/1350-4487(94)90086-8

Rhodes, E. J. (2015). Dating sediments using potassium feldspar single-grain IRSL: Initial methodological considerations. Quaternary International, 362, 14–22. https://doi.org/10.1016/j.quaint.2014.12.012

Saha, S., Owen, L. A., Orr, E. N., & Caffee, M. W. (2018). Timing and nature of Holocene glacier advances at the northwestern end of the Himalayan-Tibetan orogen. Quaternary Science Reviews, 187, 177–202. https://doi.org/10.1016/j.quascirev.2018.03.009

Salisbury, J. B., Arrowsmith, J. R., Brown, N., Rockwell, T., Akciz, S., & Ludwig, L. G. (2018). The age and origin of small offsets at van matre ranch along the san andreas fault in the Carrizo Plain, California. Bulletin of the Seismological Society of America, 108(2), 639–653. https://doi.org/10.1785/0120170162

Smedley, R. K., Duller, G. A. T., & Roberts, H. M. (2015). Bleaching of the post-IR IRSL signal from individual grains of K-feldspar: Implications for single-grain dating. Radiation Measurements, 79, 33–42. https://doi.org/10.1016/j.radmeas.2015.06.003

Wintle, A. G., & Murray, A. S. (2006). A review of quartz optically stimulated luminescence characteristics and their relevance in single-aliquot regeneration dating protocols. Radiation Measurements, 41(4), 369–391. https://doi.org/10.1016/j.radmeas.2005.11.001